Microwave-assisted synthesis and magnetic properties of M-SrFe 12 O 19 nanoparticles

Bilel Grindi, Z. Beji, G. Viau, A. Benali

Microwave-assisted synthesis and magnetic properties of M-$SrFe_{12}O_{19}$ nanoparticles

B. Grindi [a,b], Z. Beji [c], G. Viau[b,*] and A. BenAli [a,d*]

[a] Synthèse et Structure des Nanomatériaux (UR11-ES30), Faculté des Sciences de Bizerte, Université de Carthage, 7021, Jarzouna, Tunisia

[b] *Université de Toulouse, LPCNO, UMR 5215 INSA-CNRS-UPS, 135 av. de Rangueil 31077 Toulouse, France*

[c] *Centre des Recherches et des Technologies de l'Energie Technopole, Laboratoires des Nanomatériaux et Systèmes des Energies Renouvelables, B.P N°95 2050 - Hammam Lif, Tunisia*

[d] *Department of Chemistry, College of Science, Imam Abdulrahman bin Faisal University, Dammam, Saudi Arabia*

Abstract

Strontium hexaferrite nanoparticles were synthesized by a microwave-assisted hydrothermal process. The variation of structure, morphology and magnetic properties of the as-produced particles and after annealing temperatures were carefully analysed. Pure M-$SrFe_{12}O_{19}$ powders were synthesized at T = 200°C using a heating rate of 25 °C.min^{-1}. The particles exhibited a magnetic coercivity of 95 kA.m^{-1} (μ_0Hc = 0.12 T), explained by the shape of the particles that crystallized as very thin platelets with a micrometer size diameter and a very high aspect ratio in which a competition between shape and magnetocrystalline anisotropy takes place. The coercivity was strongly enhanced with Hc = 360 kA.m^{-1} (μ_0 Hc = 0.445 T) by annealing at the optimum temperature of 1000°C. In order to optimize the particle morphology and magnetic properties after annealing, the heating rate of the microwave synthesis was increased. At T = 200°C using a heating rate of 40 °C.min^{-1} the particle exhibited a size in the range 20 - 100 nm. The powder crystallized as a mixture of hexaferrite and ferrihydrite. After annealing at 1000 °C, M-$SrFe_{12}O_{19}$ with a small amount of hematite (<15 %) was obtained. The coercivity was strongly enhanced to reach the value Hc = 465 kA.m^{-1} (μ_0Hc = 0.585 T).

Key words:

Strontium hexaferrite; Nanoparticles; Micro-wave assisted synthesis; Hydrothermal; Hard magnetic materials.

Corresponding authors: A. Ben Ali, amor.benali@fsb.rnu.tn

G. Viau, gviau@insa-toulouse.fr

1. Introduction

Since their discovery in 1952 by the Philips Research Laboratory [1], the M-strontium or barium hexaferrite (SrM: $SrFe_{12}O_{19}$ or BaM: $BaFe_{12}O_{19}$) has become the most widely used material for the manufacture of permanent magnets. This is due to their high magnetocrystalline anisotropy, good saturation magnetization, excellent chemical, thermal stability and low cost [2]. These properties depend on the structure, morphology and size of the particles [3,4,5,6]. In the last few years, greatest interest was devoted to synthesize magnetic nanoparticles by the so-called "chimie douce" methods (sol-gel route, polyol process, solvothermal methods…) [7,8]. These low temperature synthesis methods make possible the elaboration of stable magnetic oxides nanoparticles (NPs) with controlled size and shape for applications in the fields of magnetic recording or biology. The size and shape of the chemically synthesized nanopowders depend on several physico-chemical parameters such as the heating rate, temperature, pH of the reaction medium, and the atmosphere in the medium. The SrM hexaferrites have been synthesized by various methods like ceramic [9,10,11], sol-gel [12,13], micellar medium [14,15], hydrothermal [16,17,18], co-precipitation [14,19,20], mechanosynthesis [21] and sonochemistry [22]. Less conventional methods of synthesis have been found like salt-assisted ultrasonic spray pyrolysis (SA-USP) method [23] or the use of microwaves synthesis like microwave-induced combustion process [24,25] and microwave-assisted calcination route [26,27].

The use of microwave for the synthesis of nanoparticles and nanostructured nanomaterials can present several interests compared to a classical heating [28]. For syntheses in polar solvent (water, polyol) the heating rate can be very high (up to $150°C.min^{-1}$) that can strongly modify the nucleation and growth steps. For syntheses in non-polar solvents (hexane, toluene), that are more or less transparent to the microwaves, a microwave assisted procedure can heat selectively the precursors [29]. The combination of microwave irradiation with hydro- or solvo-thermal conditions allows reaching ultrafast heating rates up to very high temperatures at relatively low autogenic pressures, which are favorable to access well-crystallized oxide inorganic nanocrystals under conditions [30]. This microwave assisted hydrothermal method has been studied for spinel ferrite particles with various compositions [31] and for BaM hexaferrites [32,33]. Interestingly, the aging of iron oxyhydroxides under microwave irradiation may significantly differ to classical thermal heating [34].

In the present work, quasi-pure strontium-iron oxides nanopowders were synthesized by microwave method in a single step at 200°C. The morphology, structure and magnetic properties are described. In the second step, we show that an appropriate annealing improves the hard magnetic properties of the hexaferrite powders. Finally, the particle mean size was decreased playing upon the heating rate of the microwave synthesis and as a consequence the coercivity was increased significantly.

2. Experimental details

2.1. Synthesis

Iron (III) nitrate nonahydrate $Fe(NO_3)_3.9H_2O$ (Strem Chemicals) and strontium nitrate $Sr(NO_3)_3$ (Alfa Aesar) were dissolved in demineralized water in various ratios. The obtained solution was afterwards added drop by drop, under argon atmosphere, in an aqueous sodium hydroxide NaOH. In all experiments, iron (III) concentration in the solution after mixing was fixed at 0.8 M. The molar ratio $R = Fe^{3+} / Sr^{2+}$ was fixed at 3 since lower Fe/Sr ratio significantly decreased the yield. The pH of the metal salt solutions was 0.8 and increases when sodium hydroxide was added, to reach a value in the range 7-10. The preparation of M-$SrFe_{12}O_{19}$ powders was sucessfull for pH = 10 or slightly higher than 10. At pH lower than 10 the obtained powders consist in pure or quasi pure hematite iron oxide Fe_2O_3 (Fig. S1, supplementary materials).

These solutions were subsequently transferred in a Teflon beaker EasyPrep reactor and heated for one hour in a microwave oven CEM Mars 6 (2.45 GHz, maximum power 650 W). The heating temperature was varied in the range 150-200°C and the heating rate between 12 and 40°C.min^{-1}.

After cooling, the precipitate was centrifuged, washed several times with diluted solution of acetic acid (0.1 M), demineralized water and ethanol. The resulting powder was dried at 50 °C for 12 hours. The first washing with the diluted acetic acid solution aims to remove the undesired Sr-rich phases that precipitate with the $SrFe_{12}O_{19}$ due to the excess of strontium in the starting mixture ($Fe^{3+}/Sr^{2+}<12$). The resulting powders were then annealed in air at different temperatures comprised between 500 and 1200°C.

2.2. Characterizations

The obtained powders were characterized by X-ray diffraction (XRD) on a PANalytical Empyrean diffractometer in the 2θ range 10-90°, using CoKα radiation (λ= 1.789/1.792Å). The unit cell parameters were refined by full pattern matching simulation [35] with the FULLPROF program [36]. The full width at half-maximum (FWHM) $B_e(2\theta)$ was corrected from the instrumental broadening $B_i(2\theta)$ determined on a standard Si powder according to $B(2\theta) = [B_e^2(2\theta) - B_i^2(2\theta)]^{1/2}$. X-Ray line broadening may be caused by finite crystallite size and microstrains. In order to determine the contribution of these two factors the Williamson and Hall model was followed. We plotted $B(hkl)\times\cos\theta$ vs $(2\sin\theta)$ for all the peaks of the $SrFe_{12}O_{19}$ powders pattern. When the crystallite size is the only cause of peak broadening, $B(hkl)\times\cos\theta$ is independent of $\sin\theta$. In this case the Williamson-Hall plot can be fitted by a horizontal line and the mean crystallite size is deduced from the FWHM using the Scherrer formula. In case of anisotropic crystallite a large dispersion of the $B(hkl)\cos\theta$ values is observed around a mean value. When the microstrains are also a cause of peak broadening, the slope of Williamson-Hall plot is no more zero. The microstrains are given by the slope of the $B(hkl)\times\cos\theta$ vs $(2\sin\theta)$ curve and the mean crystallite size can be calculated using the B value

extrapolated at $\theta = 0$.

The raw particles morphology was studied by transmission electron microscope (TEM) at 100 kV with JEOL JEM1011 microscope. The particles were dispersed in ethanol and sonicated, one drop of the suspension was deposited on a carbon coated copper grid and the solvent was evaporated at room temperature under vacuum. Raw and annealed powders were observed by field emission gun scanning electron microscopy (FEG-SEM) using a JEOL JSM7800F microscope. Energy Dispersive X-Ray Spectroscopy (EDS) analyses were performed using a SDD Bruker detector coupled with the SEM operating at 30 kV.

The magnetic measurements were carried out using Quantum Design Physical Property Measurement System (PPMS) in Vibrating Sample Magnetometer (VSM) configuration. Magnetization loops, M(H), were recorded at 300K with applied field varying between ± 5T. The highest field value was generally not enough to reach the magnetization saturation of the powders. The saturation magnetization values, Ms, were determined by extrapolating the M(1/H) curves to 1/H = 0.

3. Results and Discussion

One-pot microwave synthesis of M-$SrFe_{12}O_{19}$ particles

The XRD pattern of the samples prepared at a temperature higher than 200 °C using a heating rate of 25 °C.min^{-1} was indexed as pure $SrFe_{12}O_{19}$ phase (fig. 1). The power XRD pattern of the samples prepared below 200 °C with the same heating rate exhibits seven broad lines at the distances 2.538 Å, 2.447 Å, 2.227 Å, 1.963 Å, 1.710 Å, 1.497 Å and 1.465 Å (fig. 1). This second pattern is very similar to the ferrihydrite XRD pattern reported by Berquó *et al.* [37]. The ferrihydrite is a class of poorly crystalline iron oxy-hydroxide with the average composition $FeOOH \cdot x\ H_2O$ (0.2–0.4). The most described is the so-called six-line ferrihydrite (6Fh) (ICSD code: 97586) which is a mixture of two components, a defect-free and a defective phase. Both phases crystallize with a hexagonal structure with a strong disorder on the cation site occupancy [38, 39, 40]. A seventh line may appear for powder with a good crystallinity [41]. The formation of a seven-line ferrihydrite (7Fh) as intermediate phase was described by Granados-Miralles *et al.* in the hydrothermal synthesis of strontium hexaferrite [16]. Pure hexaferrite was obtained after a ripening process and progressive dissolution of the ferrihydrite particles. Our result at 150 °C confirms that a 7Fh like phase appears as an intermediate phase. The peak positions measured experimentally are consistent with the (100), (101), (102), (103), (104), (105) and (110) reflexions proposed by Drits et al. [38] of a hexagonal phase with the parameters a = 2.93 Å and c = 9.27 Å. After 1 h at 150 °C the ferrihydrite particles did not totally disappear. The temperature of 150 °C is too low for such a ripening process whereas it can take place at 200 °C.

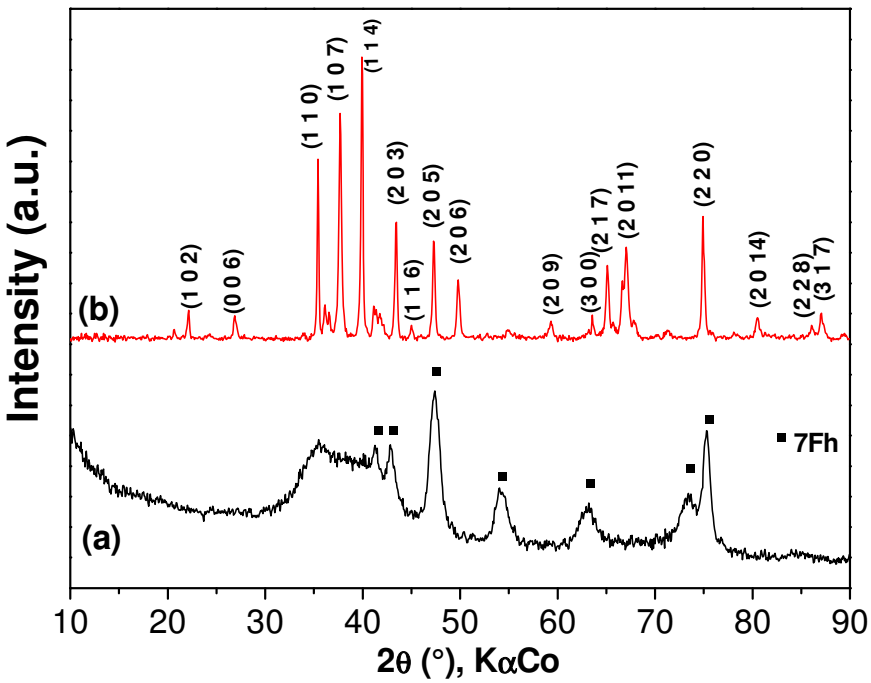

Figure 1. XRD patterns of powders obtained by microwave heating for one hour at 150°C (a) and at 200°C (b) a solution (pH = 10) of iron and strontium nitrates with a heating rate of 25°C.min^{-1}.

Morphology, structure and microstructure of the quasi-pure strontium hexaferrite $SrFe_{12}O_{19}$ powder, synthesized at 200 °C were investigated in detail. SEM and TEM analysis showed thin hexagonal platelets (Fig. 2). The particle diameter varies between 400 and 1200 nm (mean diameter D_m = 1000 nm), the mean thickness is T_m = 30 nm and the mean aspect ratio $AR_m = D_m/T_m$ = 33. Some particles tend to stack sideway forming thicker agglomerates. A typical EDS spectrum of the powder is given in the supplementary materials (Fig. S2). The experimental molar ratio Fe/Sr was equal to 11.5, very close to the $SrFe_{12}O_{19}$ stoichiometry. X-ray profile of the nanopowders has been refined by "full pattern matching" in the $P6_3/mmc$ space group using Fullprof program and leads to the following unit cell parameters $a = b$ = 5.8911 Å, c = 23.1113 Å; α = β = 90° and γ = 120°. The reliability factors were R_p = 1.26, R_{wp} = 2.09, R_{exp} = 0.67 and χ^2 = 9.67. A comparison between the experimental and simulated patterns is given in the supplementary materials, Fig. S3). The cell parameters are close to that of the reference ICDD file 01-080-1197 (a = 5.8836 Å, c = 23.0376 Å) [42]).

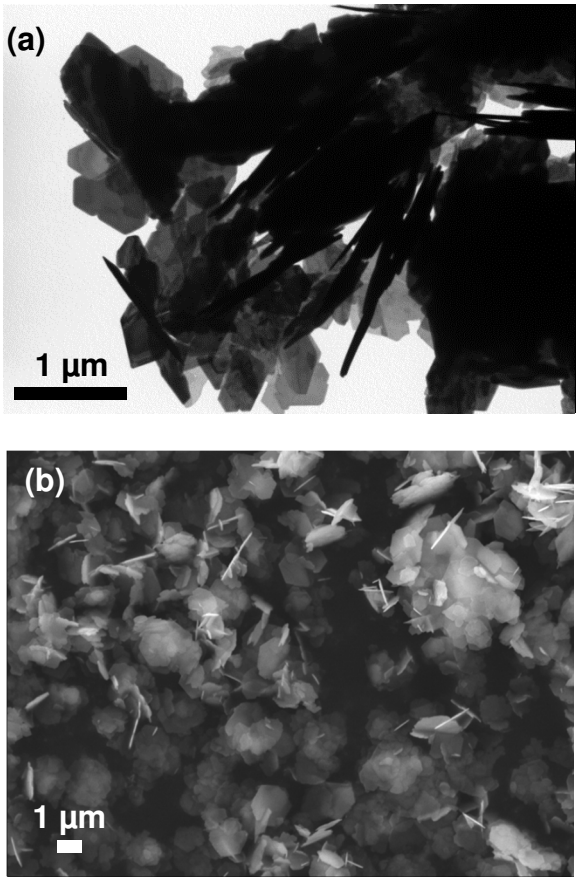

Figure 2. TEM image (a) and SEM scan image (b) of **M-**$SrFe_{12}O_{19}$ platelets.

The broadening of the XRD lines was found to strongly depend on the (hkl) indexes indicating a strong anisotropy of the crystallites. The (006) line was found broader than the (110) line revealing a smaller crystallographic coherence along the *c* axis than perpendicular to it. As the (006) line is a harmonic of the (001) line, this difference is explained by a preferential growth of the hexaferrite crystals perpendicular to the c axis. This is in agreement with the formation of platelets with the *c* axis normal to the platelets. The mean crystallite size $L_{(006)}$ calculated with the Scherrer equation was found equal to 30 nm. This value is very close to the particle mean thickness measured by TEM. The mean crystallite size $L_{(110)}$ was found equal to 90 nm. This value is lower than the particle mean diameter showing some polycrystalline platelets.

The magnetization loop M(H) at 300 K of a representative raw $SrFe_{12}O_{19}$ powder is shown in Figure 6. A fairly open hysteresis loop is observed with a coercivity $H_c = 95$ kA.m^{-1} ($\mu_0 Hc = 0.12$ T) in agreement with a ferromagnetic order and a strong magnetocrystalline anisotropy. The saturation magnetization is $M_s = 64$ A.m^2.kg^{-1} and the remanence to saturation ratio, Mr/Ms, is close to 0.5 which is the expected value for an assembly of monodomain particles randomly oriented with respect to the applied field direction. These magnetic properties are similar to that of nanoplatelets produced by conventional hydrothermal method $H_c = 84$ kA.m^{-1} ($\mu_0 Hc = 0.106$ T), $M_s = 56$ A.m^2.kg^{-1} and M_r

= 16.5 $A.m^2.kg^{-1}$ [43].

Annealing of $SrFe_{12}O_{19}$ powders

In order to improve the magnetic properties, the pure M-$SrFe_{12}O_{19}$ powders were annealed in air at a temperature comprised between 500 and 1200°C.

The particle shape variation with annealing was followed by SEM (Fig. 3). For annealing temperature up to 800°C the platelet morphology did not change dramatically. Very thin platelets were still observed on the SEM micrographs. After annealing at 1000°C, the platelet shape was retained but the platelet thickness increased (Fig. 3d) due to a beginning of sintering. The mean diameter (D_m) and thickness (T_m) measured on the SEM images are reported in Table 1. T_m increased from 30 nm to more than 100 nm at 1000°C while D_m is almost constant around 1-1.5 µm. As a consequence the mean aspect ratio exhibited a steep decrease at 1000°C (supplementary materials, Fig. S4). Above 1050°C the particles appeared totally sintered (Fig. 3e, 3f) with D_m and T_m that strongly increased (Table 1).

The XRD patterns of the annealed powders recorded at room temperature showed that the M-$SrFe_{12}O_{19}$ phase was maintained after annealing (Fig. 4). It is interesting to note that hematite appears as a secondary phase for the annealing temperature range of 500-950°C that may result of the crystallization of a minor amorphous phase present in the raw powder. The relative amount of hematite was found equal to 4% at 500°C and decreases progressively at higher temperature (3% at 900°C, 1% at 950°C) and finally disappears totally at 1000°C (Fig. 4) certainly due to the formation of a solid solution with the hexaferrite phase.

The parameters *a* and *c* of the M-$SrFe_{12}O_{19}$ phase extracted from the Rietveld refinements are reported in Table 1. *a* and *c* decrease steadily when the annealing temperature increases in the range 500-1000°C and increases for calcination temperature above 1000°C (Tab. 1). The maximum contraction of the lattice parameters was observed after annealing at 1000°C with $\Delta a/a_{raw}$ = - 0.044 %, $\Delta c/c_{raw}$ = - 0.172%. and $\Delta(c/a)$ = - 0.127 %.

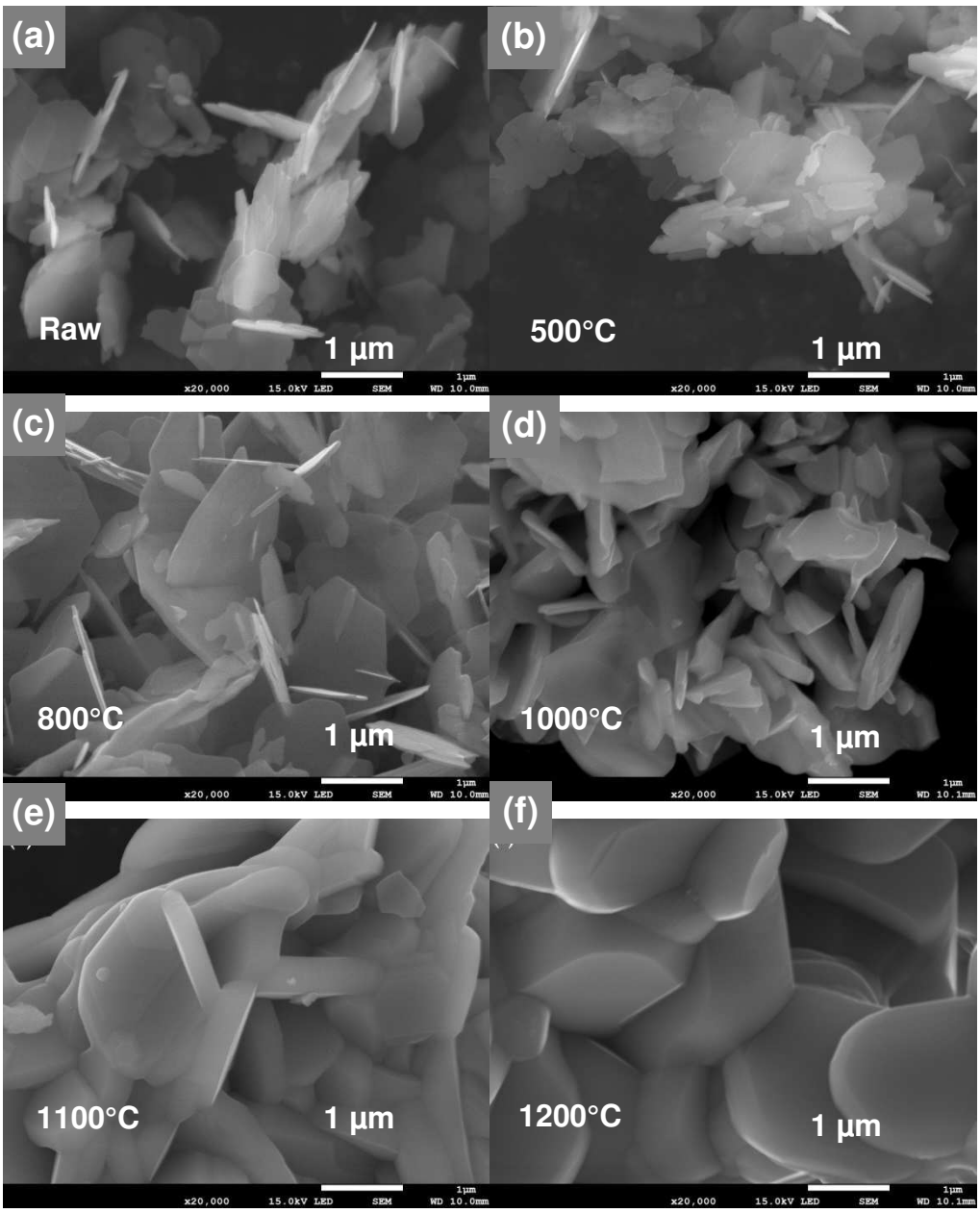

Figure 3. SEM images of M-$SrFe_{12}O_{19}$ powders As-prod (a) and annealed for 1 h at 500°C (b), 800°C (c), 1000°C (d), 1100°C (e) and 1200°C (f).

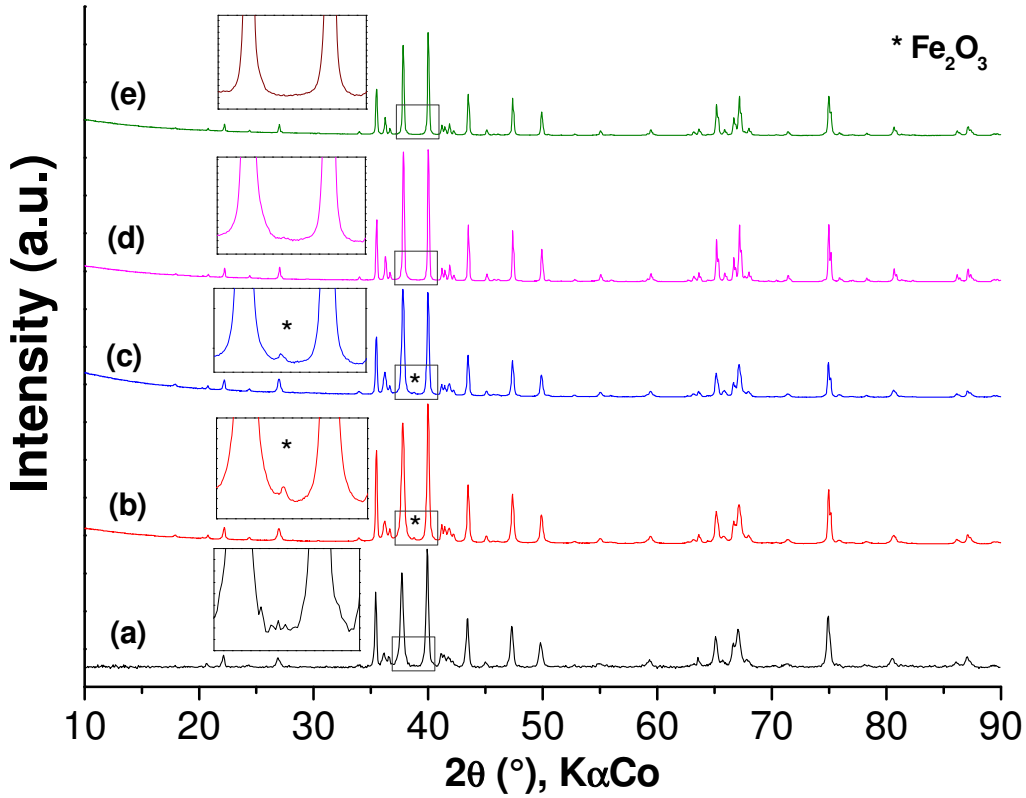

Figure 4. X-ray diffraction patterns of the M-$SrFe_{12}O_{19}$ powders annealed for one hour at various temperatures (a) 25°C, (b) 500°C, (c) 800°C, (d) 1000°C and (e) 1200°C. *Inset*: zoom in the 2θ range 37-41°.

The microstructure of the M-$SrFe_{12}O_{19}$ phase was analysed according to the Williamson and Hall model. The Williamson-Hall plots for different annealing temperatures are given in Figure 5 and in supplementary materials. For the annealing temperatures in the range 500-1050°C the Williamson-Hall plots were fitted by a horizontal line, showing that the contribution of the microstrains to the peak broadening could be neglected. Moreover, for this annealing temperature range, a large dispersion around the mean B×cosθ value was observed which is the feature of crystallite anisotropy (Fig. 5a and supplementary materials, Fig. S5). The mean crystallite sizes $L_{(006)}$ and $L_{(110)}$ were calculated from the (006) and (110) reflexion broadening (Tab. 1). The crystallite anisotropy calculated as the ratio $L_{(110)}/L_{(006)}$ decreased with increasing annealing temperature with the main drop observed between 1000 and 1050°C (supplementary materials, Fig. S6). The crystallite anisotropy almost disappears for the annealing temperature of 1050°C (Fig. 5b). Above 1100°C the slope of the Williamson–Hall plots was no more zero, indicating a significant contribution of the microstrains to the peak broadening (Fig. 5c). The microstrains and the mean crystallite size, L_m, calculated using the B value extrapolated at $\theta = 0$, increased when the temperature increased from 1100°C to 1200°C (Tab. 1).

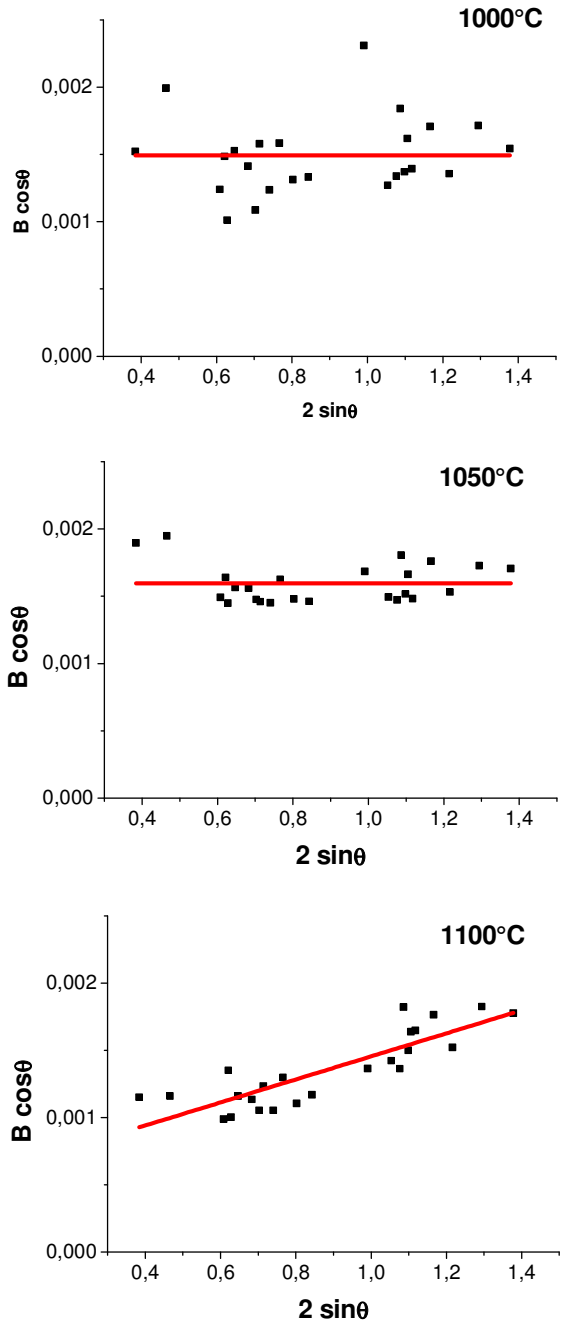

Figure 5. Williamson-Hall plot of M-$SrFe_{12}O_{19}$ powders prepared by microwave heating and annealed for one hour at temperature between 1000-1100°C.

Temperature (°C)	a (Å)	c (Å)	D_m (μm)	T_m (nm)	L_m (nm)	$L_{(006)}$ (nm)	$L_{(110)}$ (nm)	ε
25	5.8868	23.0914	1.0	30	52	30	90	0
500	5.8867	23.0800	1.0	30	42	30	65	0
800	5.8866	23.0721	1.4	50	48	35	75	0
900	5.8865	23.0605	1.5	60	70	40	80	0
950	5.8856	23.0541	1.5	60	82	50	95	0
1000	5.8841	23.0515	1.5	130	115	70	130	0
1050	5.8839	23.0522	1.5	170	105	80	110	0
1100	5.8836	23.0565	2.0	350	300	-	-	$9 \bullet 10^{-4}$
1200	5.8838	23.0608	4.5	800	402	-	-	$15 \bullet 10^{-4}$

Table 1. Crystallographic parameters, particle mean diameter (D_m) and thickness (T_m), (from SEM microscope) mean crystallite size, L_m, and calculated for the (006) and (110) reflexions, $L_{(006)}$ and $L_{(110)}$ (from Rietveld refinement) of a M-$SrFe_{12}O_{19}$ powder annealed for one hour at different temperatures.

The magnetization curves of the M-$SrFe_{12}O_{19}$ obtained powders, annealed at different temperatures, were measured at room temperature (Fig. 6). The variation of the saturation magnetization and the coercivity of the powders annealed at different temperatures are plotted in figure 7. The saturation magnetization steadily increased when the calcination temperature was increased. This variation can be interpreted by an improvement of crystallinity after annealing at high temperature and a crystallite growth leading to a higher magnetic order within and at the surface of the particles. Nevertheless, even after annealing at 1000 °C the magnetization did not reach the saturation under the magnetic field of 5 T. The easy axes are randomly oriented with respect to the direction of the applied field. As the particles exhibit very strong magnetocrystalline anisotropy, very high field are required to saturate the particles oriented along their hard axis. This can explain the difficulty to saturate the random powders. The saturation magnetization value was extrapolated at high fields. After annealing at 1000 °C, Ms was 76 $A.m^2.kg^{-1}$ which is equal to that of single crystal prepared by the ceramic route [9]. The coercivity was almost constant for annealing temperature up to 800°C and then strongly increases to reach a maximum value of 360 $kA.m^{-1}$ ($\mu_0 Hc = 0.455$ T) for T = 1000 °C. Annealing at higher temperatures provoked a strong decrease of coercivity down to a value close to that of the raw powder (Fig. 7).

The variation of the magnetic properties with the annealing temperature is consistent with the morphological and crystallite changes. M-$SrFe_{12}O_{19}$ particles exhibit very high uniaxial magnetocrystalline anisotropy with the *c* axis the magnetic easy axis [44]. The magnetic properties of small particles strongly depend on the particle size and shape. For the as-produced very thin platelets a competition between magnetocrystalline anisotropy and shape anisotropy is expected since the magnetocrystalline anisotropy tends to favour a spontaneous magnetization parallel to the *c* axis while the shape anisotropy tends to favour a magnetization in the plane of the platelets to minimize the demagnetizing effects. This effect may explain the low coercivity measured on the raw hexaferrite particles. When the annealing temperature was increased the particle and the crystallite lose their anisotropy explaining the increase of the magnetic coercivity. The optimum annealing temperature for the coercivity increase is around 1000°C. The coercivity decreasing at higher temperatures can be explained by a size increase above the critical size corresponding to the transition from a magnetic single-domain to a poly-domain configuration [2].

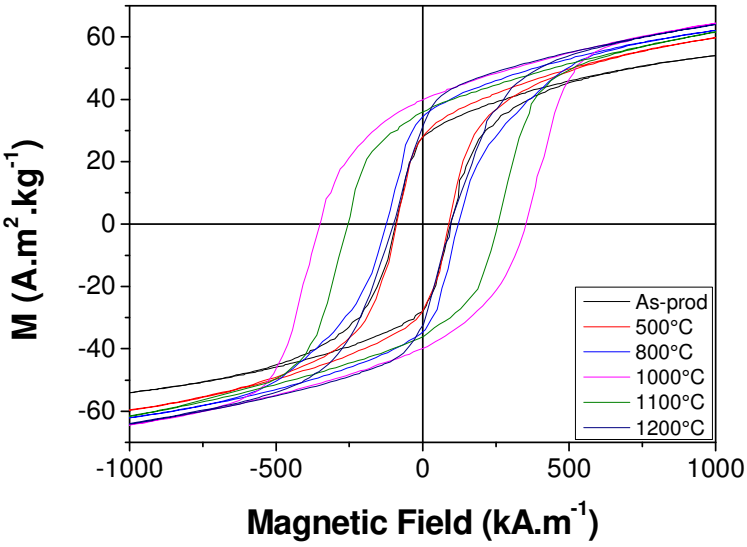

Figure 6. Magnetization curve of M-$SrFe_{12}O_{19}$ powders, raw and annealed for 1h at various temperatures.

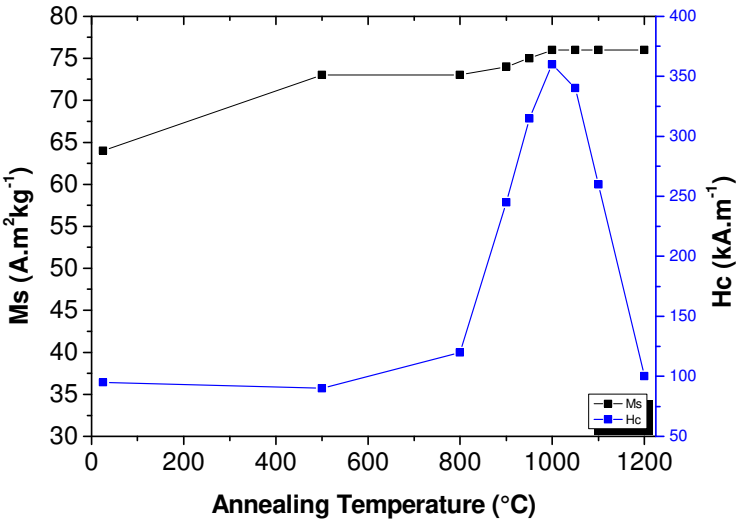

Figure 7. Variation of saturation magnetization and coercivity of M-$SrFe_{12}O_{19}$ powders annealed for 1h at different temperatures.

Influence of microwave heating rate

The heating rate was varied in the range 12-40 °C.min^{-1}. With heating rate below 25 °C.min^{-1} mixtures of hexaferrite and hematite (α-Fe_2O_3) were obtained (Fig. S7). Hematite crystallization was also observed using a classical hydrothermal process with the same experimental parameters. Hematite formation was avoided thanks to the high heating rate available with the microwave. High heating rate also change the nucleation and growth steps. The particles produced by the microwave-assisted hydrothermal route with a heating rate of 40 °C.min^{-1} exhibit a much lower mean size than those prepared at 25 °C.min^{-1}. Very thin platelets with a diameter in the range 20-100 nm were observed by electron microscopy (Fig. 8a). The thickness of the small platelets viewed sideways was found between 5 and 10 nm. The molar ratio Fe/Sr measured by EDS on the powder was found equal to 11.7. Despite a global composition very close to the stoichiometry of the hexaferrite, the XRD pattern of the as-produced powder revealed a mixture of M-$SrFe_{12}O_{19}$ and a 7Fh like phase (Fig. 8b). The saturation magnetization of the as-produced particles was found Ms = 13 A.m^2.kg^{-1}. This value is much lower than that measured on the pure hexaferrite prepared with a heating rate of 25 °C.min^{-1} (Ms = 64 A.m^2.kg^{-1}). Previous studies showed that the ferrihydrite phase is antiferromagnetic [39]. The weak magnetization is consistent with a mixture of a M-$SrFe_{12}O_{19}$ particles with antiferromagnetic ferrihydrite-like particles. From this value the mass percentage of M-$SrFe_{12}O_{19}$ in the mixture can be roughly estimated at 20 %.

The XRD pattern of the powder annealed at 1000 °C revealed a mixture of M-$SrFe_{12}O_{19}$ and hematite (Fig. 8b). The relative amount of hematite, in mass percentage, was estimated by Rietveld analysis at 15 %. This amount is much lower than the estimated one of 7Fh phase in the as-produced powder. It

suggests that the main part of the ferrihydrite-like particles transform into M-$SrFe_{12}O_{19}$ particles at high temperature.

After annealing at 1000 °C, the powder exhibited grains with an isotropic shape contrary to platelet-shaped particles of pure hexaferrite prepared with the heating rate of 25 °C.min^{-1} and annealed in the same conditions (Fig. 3d). The grain size measured on the SEM images was found in the range 300-500 nm (Fig. 8c).

The saturation magnetization determined by extrapolation at high field was found equal to Ms = 64 A.m^2.kg^{-1}. This value is consistent with a powder that consisted in 85 % of M-$SrFe_{12}O_{19}$ with a saturation magnetization of 76 A.m^2.kg^{-1} (i.e. the value determined on pure M-$SrFe_{12}O_{19}$ annealed at 1000 °C) and 15 % of antiferromagnetic hematite with a negligible saturation magnetization, so in very good agreement with the Rietveld analysis. The magnetization loop of the powder annealed at 1000 °C exhibited a coercivity Hc = 465 kA.m^{-1} (5850 Oe). This value is much higher than the coercivity of the powder prepared with the heating rate of 25 °C.min^{-1} and annealed in the same conditions. This result is explained by the strong difference of the powder microstructure when the starting particle size and shape were modified by changing the microwave heating rate.

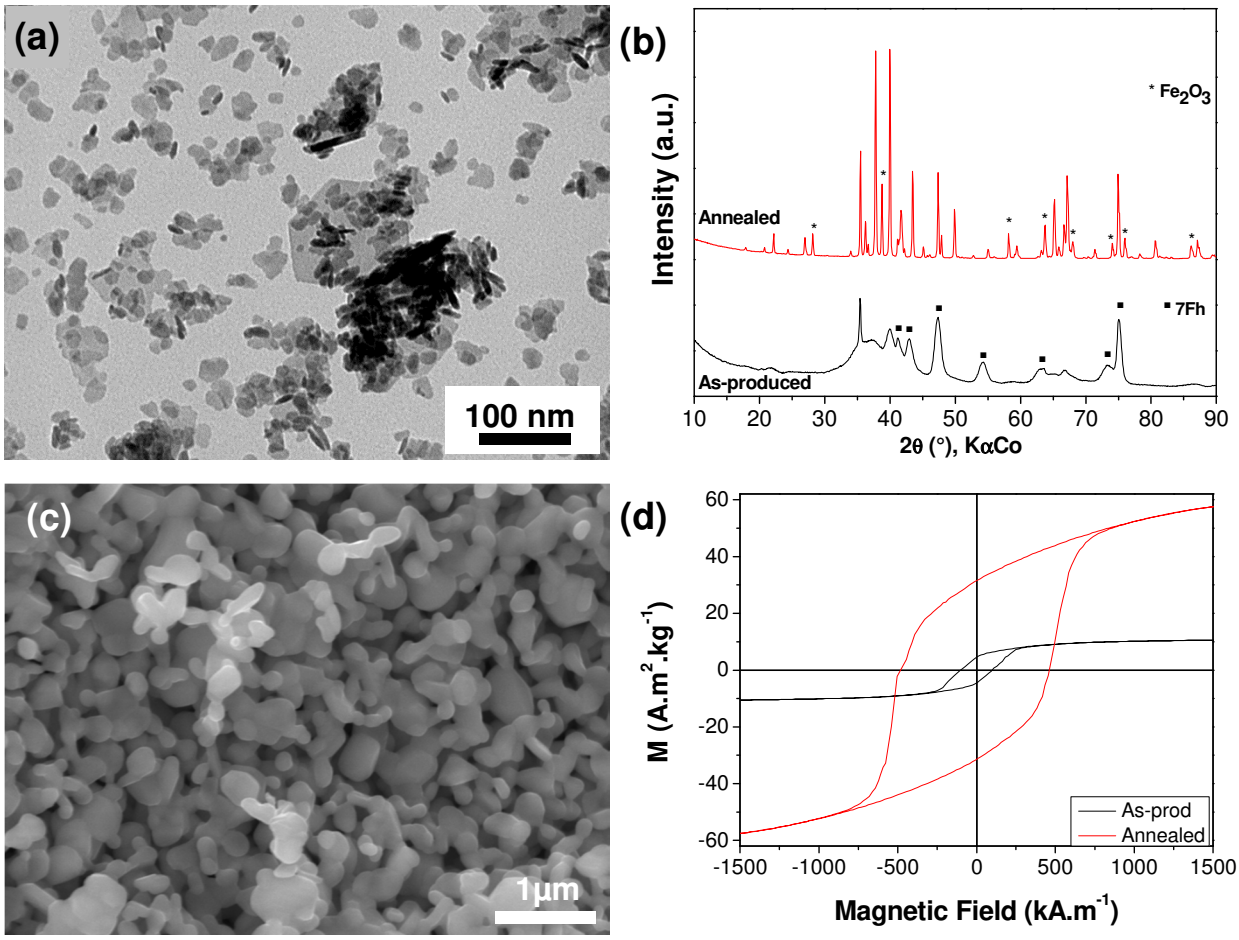

Figure 8. (a) TEM image of nanoparticles obtained by heating at 200 °C for 1 h of a solution containing iron and strontium nitrates (pH = 10) with heating rate 40°C.min^{-1}; (b) SEM image of the same particles annealed at 1000 °C for 1 h; (c) XRD pattern of the as-produced and annealed powders ; (d) Magnetization curve of powders before and after annealing.

4. Conclusion

This study showed that pure strontium hexaferrite M-$SrFe_{12}O_{19}$ can be obtained in a single step synthesis by microwave heating in hydrothermal conditions at 200 °C with a heating rate of 25 °C.min^{-1}. In the same experimental conditions at the same temperature classical hydrothermal synthesis gave a mixture of hexaferrite M-$SrFe_{12}O_{19}$ and hematite α-Fe_2O_3. With the microwave-assisted hydrothermal process hematite crystallization was avoided thanks to a high heating rate. The other interest of the microwave-assisted hydrothermal method compared to the classical hydrothermal one is to reduce considerably the reaction time. The particles crystallized as very thin platelets with a very large aspect ratio. This shape induced a competition between the shape and magnetocrystalline anisotropy that limited the coercivity of the M(H) loop to only 95 KA.m^{-1} (μ_0Hc = 0.12 T). The coercivity was enhanced by annealing at 1000°C. This temperature is optimum because the particle

shape anisotropy was strongly reduced. At higher temperature microstrains appeared and the particle growth due to sintering caused a strong decreasing of the coercivity.

The heating rate had a strong influence on the particle size and composition. While pure M-$SrFe_{12}O_{19}$ particles were obtained with a heating rate of 25 °C.min^{-1} a mixture of M-$SrFe_{12}O_{19}$ and ferrihydrite (7Fh) was observed when the heating rate was increased to 40 °C.min^{-1}. The particle size decreased to the range 20-100 nm instead of 100 nm – 1µm for the particles prepared with a heating rate of 25 °C.min^{-1}. The powder prepared using a heating rate of 40 °C.min^{-1} exhibited a weak saturation magnetization due to the large amount of ferrihydrite particles. After annealing at 1000 °C, these powders combined a high saturation magnetization thanks to a limited amount of hematite (15 %) and a very high coercivity thanks to optimized particles size and shape.

The perspective of this work is to analyse in details the nature of the ferrihydrite phase and to explore the effects of higher heating rates on the particle structure and morphology in order to take additional advantages of the microwave heating for the preparation of particles with higher coercivity.

References

[1] J. Smit, H.P.J. Wijn, Ferrites (Philips Technical Library) Eindhoven, Netherland 1959

[2] O. Gutfleisch, M. A. Willard, E. Brück, C. H.Chen, S. G. Sankar, J. P. Liu, Magnetic Materials and Devices for the 21st Century: Stronger, Lighter, and More Energy Efficient, Adv. Mater. 23 (2011) 821-842.

[3] R.C. Pullar, Hexagonal ferrites: A review of the synthesis, properties and applications of hexaferrite ceramics, Prog. Mater Sci. 57 (2012) 1191-1334.

[4] A. Ataie and S. Heshmati-Manesh, Synthesis of ultra-fine particles of strontium hexaferrite by a modified co-precipitation method, J. Eur. Ceram. Soc. 21 (2001) 1951-1955.

[5] D.-H. Chen and Y.-Y. Chen, Synthesis of strontium ferrite nanoparticles by coprecipitation in the presence of polacrylic acid, Mater. Res. Bull. 37 (2002) 801-810.

[6] P. Karipoth, A. Thirumurugan, S. Velaga, J.-M. Greneche, R. Justin Joseyphus, Magnetic properties of FeCo alloy nanoparticles synthesized through instant chemical reduction, J. App. Phys. 120 (2016) 123906.

[7] M. A. Willard, L. K. Kurihara, E. E. Carpenter, S. Calvin,V. G. Harris, Chemically prepared magnetic nanoparticles, Int. Mater. Rev. 49 (2004) 125-170.

[8] F.N. Tenorio Gonzalez, A.M. Bolarín Miró, F. Sánchez De Jesús, C.A. Cortés Escobedo, S. Ammar, Mechanism and microstructural evolution of polyol mediated synthesis of nanostructured M-type $SrFe_{12}O_{19}$, J. Magn. Magn. Mater. 407 (2016) 188-194.

[9] H. Kojima, Fundamental properties of hexagonal ferrites with magnetoplumbite structure, in Ferromagnetic Material, Vol 3 (ed E.P. Wohlfarth), North Holland, Amsterdam, The Netherlands, 1982.

[10] S.A. Seyyed Ebrahimi, A. Kianvash, C.B. Ponton, I.R. Harris, The effect of hydrogen on composition, microstructure and magnetic properties of strontium hexaferrite, Ceram. Int. 26 (2000) 379-381.

[11] H.R. Koohdar, S.A. Seyyed Ebrahimi, A. Yourdkhani, R. Dehghan, F. Zajkaniha, Optimization of hydrogen dynamic heat treatment and re-calcination for preparation of strontium hexaferrite nanocrystalline powder, J. Alloys Compd. 479 (2009) 638-641.

[12] C-J. Li, G-R Xu, Template preparation of strontium hexaferrite ($SrFe_{12}O_{19}$) micro/nanostructures: Characterization, synthesis mechanism and magnetic properties Mater. Res. Bull. 46 (2011) 119-123.

[13] Z. Durmus, H. Sozeri, M.S. Toprak, A. Baykal, Effect of Fuel on the Synthesis and Properties of Poly(methyl methacrylate) Modified $SrFe_{12}O_{19}$ Nanoparticles, J. Supercond. Nov. Magn. (2012)

1957-1963.
[14] A. Drmota, M. Drofenik, A. Znidarsic, Synthesis and characterization of nano-crystalline strontium hexaferrite using the co-precipitation and microemulsion methods with nitrate precursors, Ceram. Int. 38 (2012) 973-979.
[15] V. Harikrishnan, P. Saravanan, R. Ezhil Vizhi, D.Rajan Babu, V.T.P. Vinod, P. Kejzlar, M. Černík, Effect of annealing temperature on the structural and magnetic properties of CTAB-capped $SrFe_{12}O_{19}$ platelets, J. Magn. Magn. Mater. 401 (2016) 775-783.
[16] C. Granados-Miralles, M. Saura-Múzquiz, E. D. Bøjesen, K. M. Ø. Jensen, H. L. Andersen and M. Christensen, Unraveling structural and magnetic information during growth of nanocrystalline $SrFe_{12}O_{19}$, J. Mater. Chem. C 4 (2016) 10903-10913.
[17] J. H. Lee, H. S. Kim, C. W. Won, Magnetic properties of strontium ferrite powder made by hydrothermal processing, J. Mater. Sci. Lett. 15 (1996) 295-297.
[18] X. Tang, R.Y. Hong, W.G. Feng, D. Badami, Ethylene glycol assisted hydrothermal synthesis of strontium hexaferrite nanoparticles as precursor of magnetic fluid, J. Alloys Compd. 562 (2013) 211-218.
[19] M.M. Hessien , M.M. Rashad, K. El-Barawy, Controlling the composition and magnetic properties of strontium hexaferrite synthesized by co-precipitation method, J. Magn. Magn. Mater. 320 (2008) 336–343
[20] I.A. Auwal, H. Erdemi, H. Sözeri, H. Güngüneş, A. Baykal, Magnetic and dielectric properties of Bi^{3+} substituted $SrFe_{12}O_{19}$ hexaferrite, J. Magn. Magn. Mater. 412 (2016) 69-82.
[21] S.V. Ketov, Yu.D. Yagodkin, A.L. Lebed, Yu.V. Chernopyatova, K. Khlopkov, Structure and magnetic properties of nanocrystalline $SrFe_{12}O_{19}$ alloy produced by high-energy ball milling and annealing, J. Magn. Magn. Mater. 300 (2006) e479-e481.
[22] R.L. Palomino, A.M. Bolarín Miró, F.N. Tenorio, F. Sánchez De Jesús, C.A. Cortés Escobedo, S. Ammar, Sonochemical assisted synthesis of $SrFe_{12}O_{19}$ nanoparticles, Ultrason. Sonochem. 29 (2016) 470-475.
[23] G.-H. An, T-Y Hwang, Y-H Choa, K Shin, Synthesis of Size-Controlled $SrFe_{12}O_{19}$ Using Modified Spray Pyrolysis–Calcination Method and Their Magnetic Properties, J. Electron. Mater. 43 (2014) 3574-3581.
[24] M. Ghobeiti Hasab, S.A. Seyyed Ebrahimi, A. Badiei, An investigation on physical properties of strontium hexaferrite nanopowder synthesized by a sol–gel auto-combustion process with addition of cationic surfactant, J. Eur. Ceram. Soc. 27 (2007) 3637-3640.
[25] M. Ghobeiti Hasab, S.A. Seyyed Ebrahimi, A. Badiei, Effect of different fuels on the strontium hexaferrite nanopowder synthesized by a surfactant-assisted sol–gel auto-combustion method, J. Non-Cryst. Solids 353 (2007) 814-816.

[26] W. Zhanyong, Z. Liuming, L. Jieli, Q. Huichun, Z. Yuli, F. Yongzheng, J. Minglin, X. Jiayue, Microwave-assisted synthesis of $SrFe_{12}O_{19}$ hexaferrites, J. Magn. Magn. Mater. 322 (2010) 2782-2785.
[27] K. Samikannu, J. Sinnappan, S. Mannarswamy, T. Cinnasamy, K. Thirunavukarasu, Synthesis and Magnetic Properties of Conventional and Microwave Calcined Strontium Hexaferrite Powder, Mat. Sci. App. 2 (2011) 638-642.
[28] I. Bilecka, M. Niederberger, Microwave chemistry for inorganic nanomaterials synthesis, Nanoscale 2 (2010) 1358-1374.
[29] E. Muthuswamy, A. S. Iskandar, M. M. Amador, S. M. Kauzlarich, Facile Synthesis of Germanium Nanoparticles with Size Control: Microwave versus Conventional Heating, Chem. Mater. 25 (2013) 1416-1422.
[30] M. Baghbanzadeh, L. Carbone, P. D. Cozzoli, C. O. Kappe, Microwave-Assisted Synthesis of Colloidal Inorganic Nanocrystals, Angew. Chem. Int. Ed. 50 (2011) 11312-11359.
[31] S. Komarneni, R. Roy, Q.-H. Li, Microwave-hydrothermal synthesis of ceramic powders, Mater. Res. Bull. 27 (1992) 1393-1405.
[32] T. Yamauchi, Y. Tsukahara, T. Sakata, H. Mori, T. Chikata, S. Katoh, Y. Wada, Barium ferrite powders prepared by microwave-induced hydrothermal reaction and magnetic property J. Magn. Magn. Mater. 321 (2009) 8-11.
[33] K. Sadhana, K. Praveena, S. Matteppanavar, B. Angadi, Structural and magnetic properties of nanocrystalline $BaFe_{12}O_{19}$ synthesized by microwave-hydrothermal method, Appl. Nanosci. 2 (2012) 247-252.
[34] M.-n. Lu, R.P. Das, W. Li, J.–h. Peng, L.-b. Zhang, Microwave mediated precipitation and aging of iron oxyhydroxides at low temperature for possible hydrometallurgical applications, Hydrometallurgy 134–135 (2013) 110-116.
[35] H.M. Rietveld, A profile refinement method for nuclear and magnetic structures, J. Appl. Crystallogr. 2 (1969) 65-71.
[36] J.R. Carvajal, Computer Program FullProf and WinPLOTR, Laboratoire Léon Brillouin CEA-CNRS, Grenoble 1998.
[37] T. S. Berquó, S. K. Banerjee, R. G. Ford, R. L. Penn, T. Pichler, High crystallinity Si-ferrihydrite: An insight into its Néel temperature and size dependence of magnetic properties J. Geophys. Res. 112, (2007) B02102.
[38] V. A. Drits, B. A. Sakharov, A. L. Salyn, A. Manceau, Structural model for ferrihydrite, Clay Minerals, 28 (1993) 185-207.

[39] E. Jansen, A. Kyek, W. Schafer, U. Schwertmann, The structure of six-line ferrihydrite, Appl. Phys. A, **2002**, *74*, S1004-S1006.

[40] A. Manceau, Am. Mineral., 96 (2011) 521–533,

[41] A. Manceau, S. Skanthakumar, L. Soderholm, PDF analysis of ferrihydrite: Critical assessment of the under-constrained akdalaite model, Am. Mineral., 99 (2014) 102–108.

[42] K. Kimura, M. Ohgaki, K. Tanaka, H. Morikawa, F. Marumo, Study of the bipyramidal site in magnetoplumbite-like compounds, $SrM_{12}O_{19}$ (M = Al, Fe, Ga), J. Solid State Chem. 87 (1990) 186-194.

[43] M. Jean, V. Nachbaur, J. Bran, J.-M. Le Breton, Synthesis and characterization of $SrFe_{12}O_{19}$ powder obtained by hydrothermal process, J. Alloys Compd. 496 (2010) 306-312.

[44] S.V. Ketov, Yu. D. Yagodkin, V.P. Menushenkov, Structure and magnetic properties of strontium ferrite anisotropic powder with nanocrystalline structure, J. Alloys Compd. 509 (2011) 1065-1068.

SUPPORTING INFORMATION

Microwave-assisted synthesis and magnetic properties of M-$SrFe_{12}O_{19}$ nanoparticles

B. Grindi [a,b], Z. Beji [c], G. Viau [b] and A. BenAli [a]

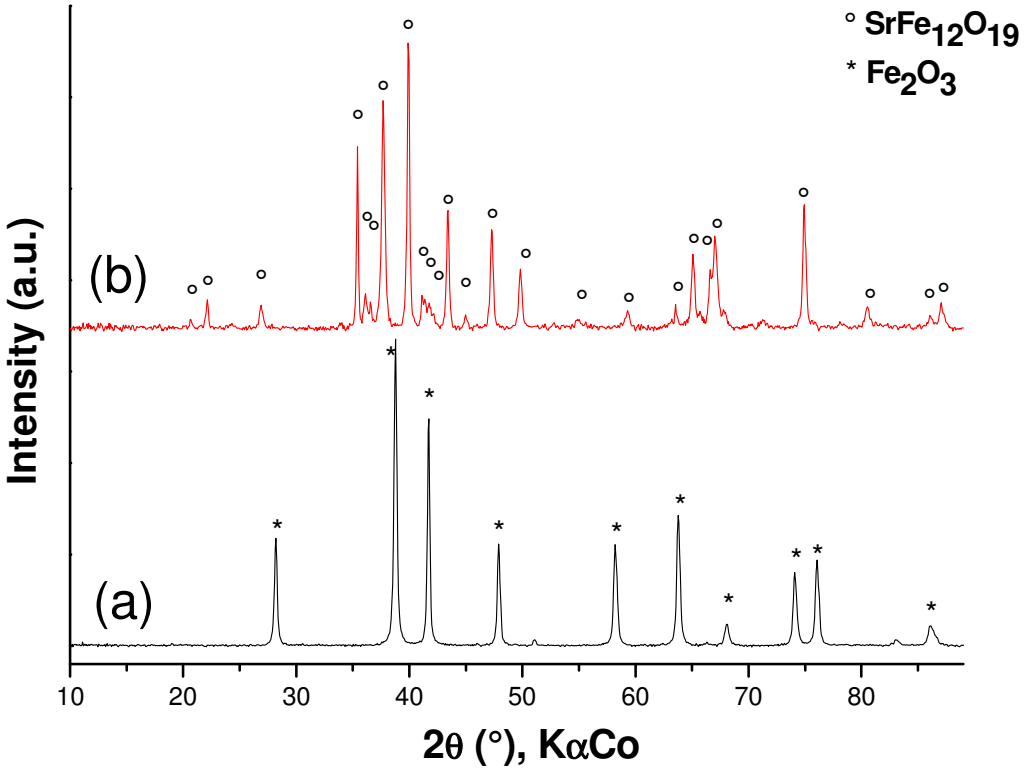

Figure S1: XRD of powders by microwave assisted synthesis obtained by heating at 200°C for 1h (heating rate 25°C.min^{-1}) a solution containing iron and strontium nitrates ([Fe^{3+}] = 0.8 M, Fe/ Sr = 3) at different pH (a) pH =7 and (b) pH=10.

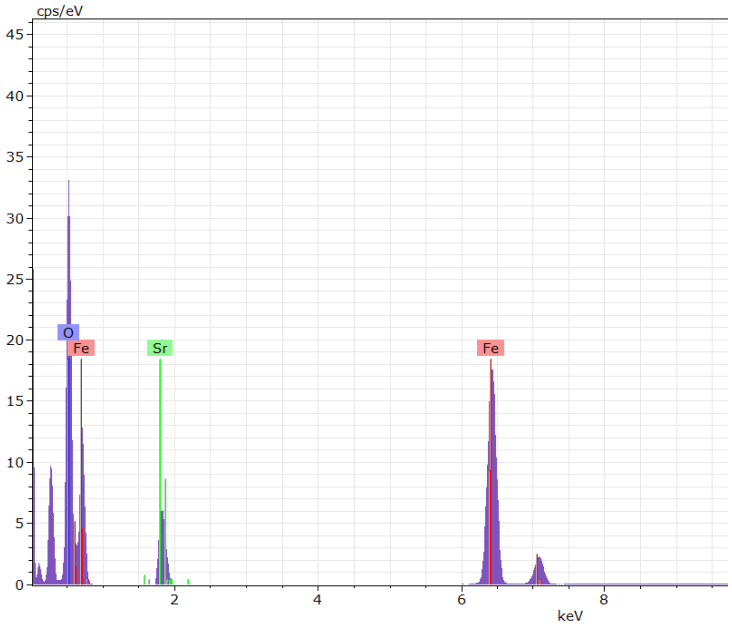

Figure S2: Energy Dispersive Spectrum of M-$SrFe_{12}O_{19}$ nanoparticles obtained by heating a solution (pH = 10) containing iron and strontium nitrates ($[Fe^{3+}]$ = 0.8 M, molar ratioFe^{3+} / Sr^{2+} = 2) at 200°C for 1h (heating rate 25 °C.min^{-1}).

The EDS analysis showed that the powders that crystallized with the hexaferrite structure do not contain other chemical element than strontium, iron, oxygen and carbon that comes from the conductive tape used to fix the powder.

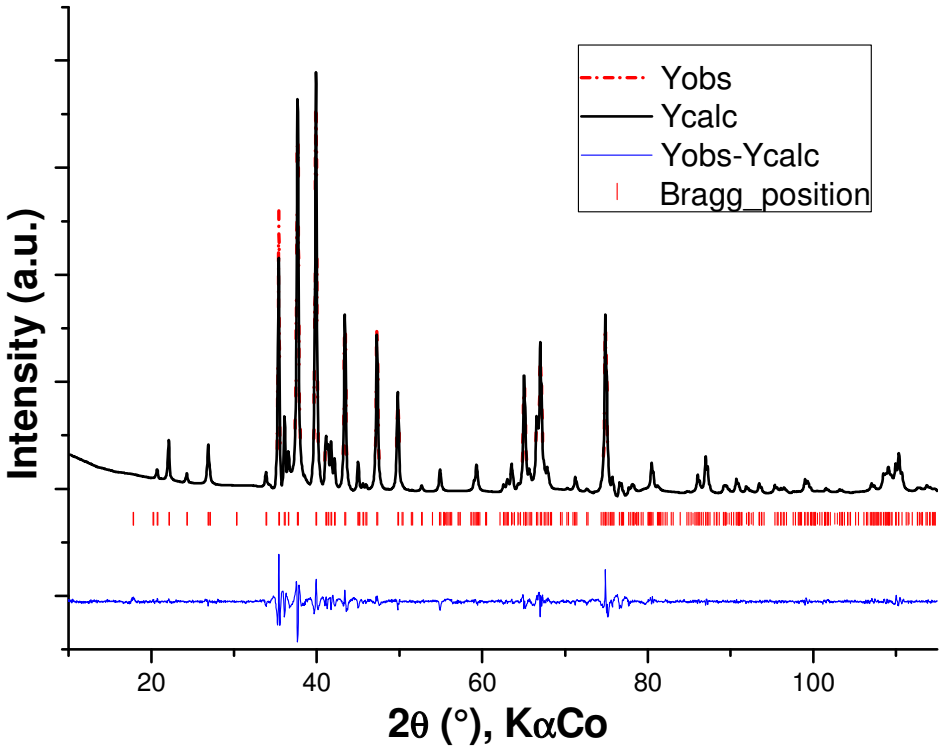

Figure S3: X-ray diffraction patterns of M-$SrFe_{12}O_{19}$ nanoparticles prepared by microwave assisted hydrothermal method at 200 °C (heating rate 25°C.min^{-1}). Experimental (red dots), simulated (black line) and difference (blue line).

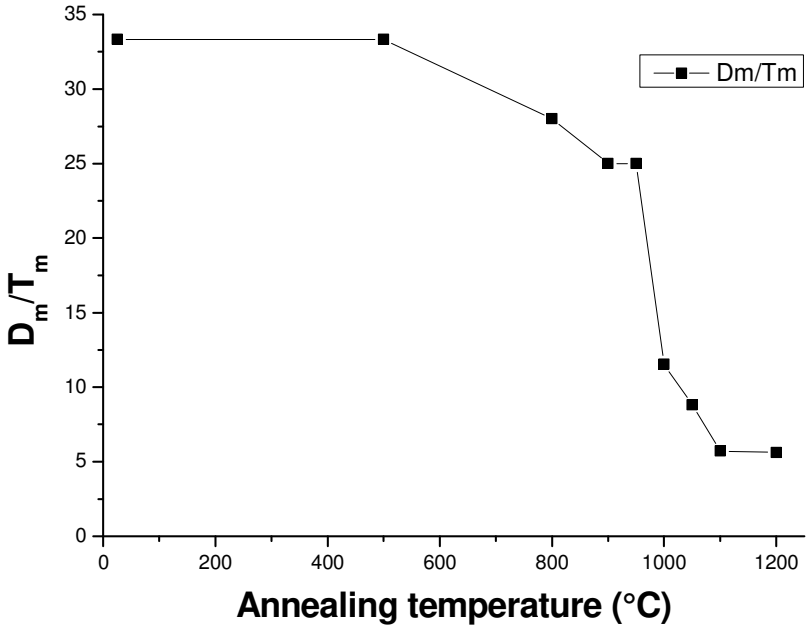

Figure S4. Mean aspect ratio, calculated as the ratio between the mean diameters D_m over the mean thickness T_m, of a M-$SrFe_{12}O_{19}$ powder as a function of the annealing temperature.

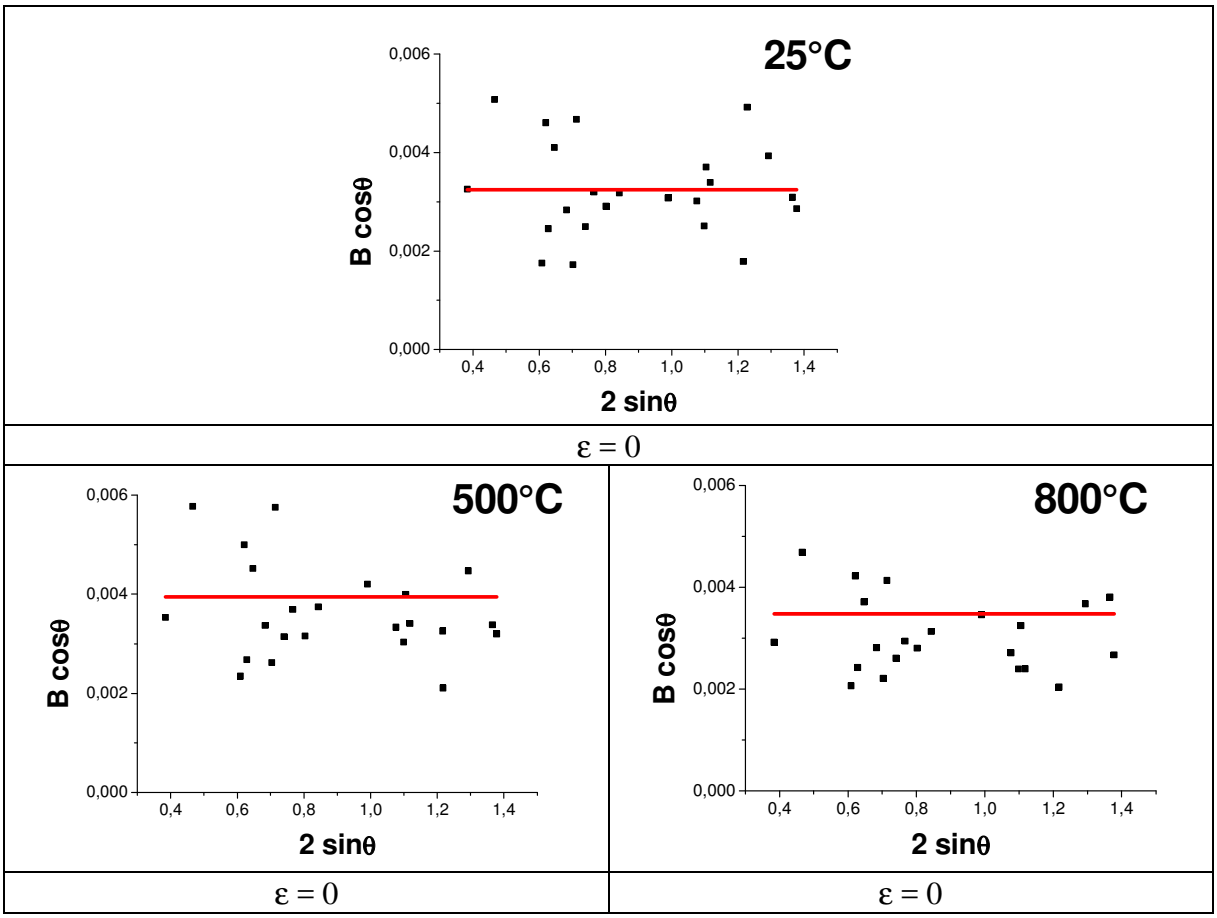

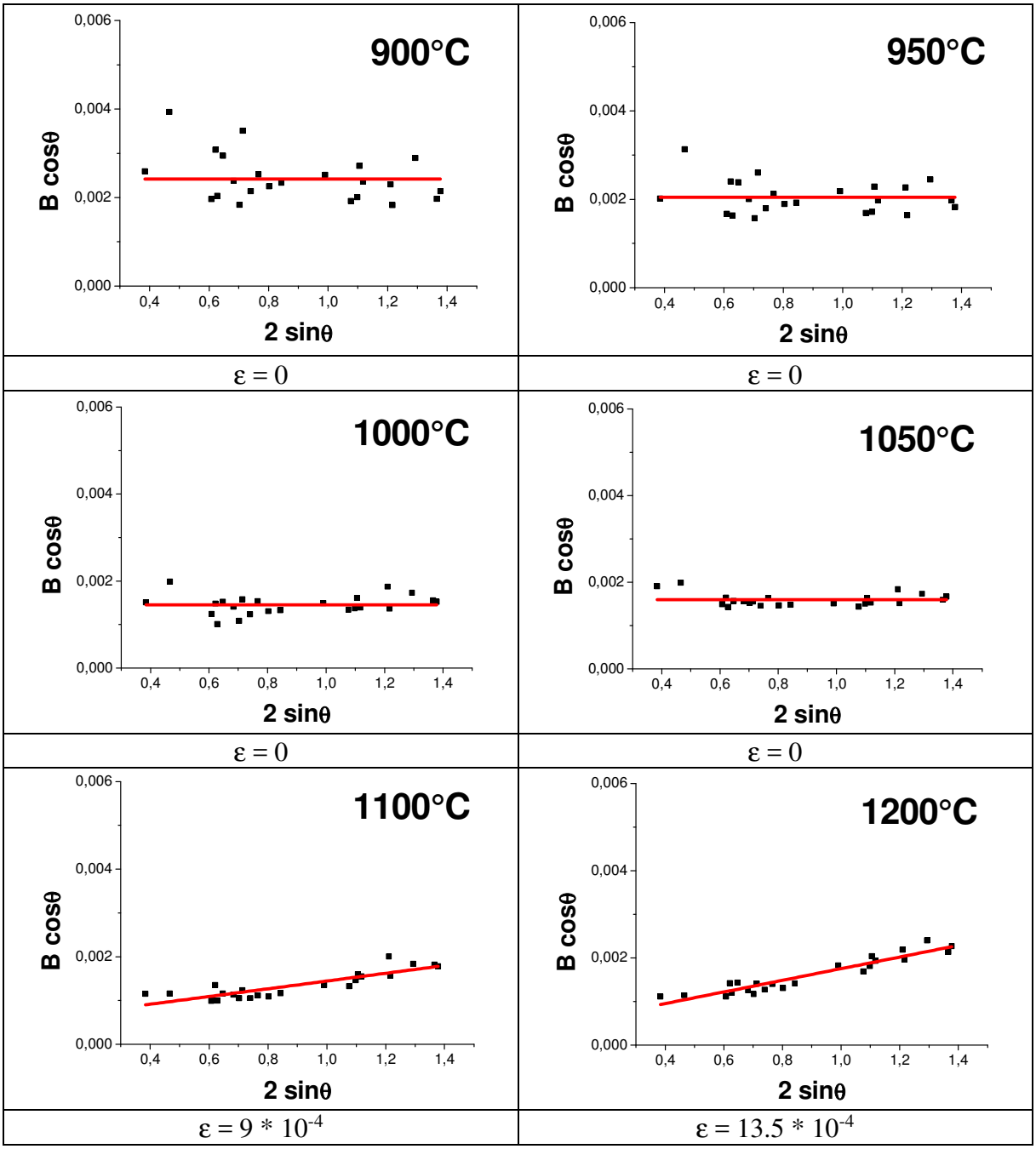

Figure S5: Williamson-Hall Plot of XRD $SrFe_{12}O_{19}$ powders annealed for one hour at different temperatures.

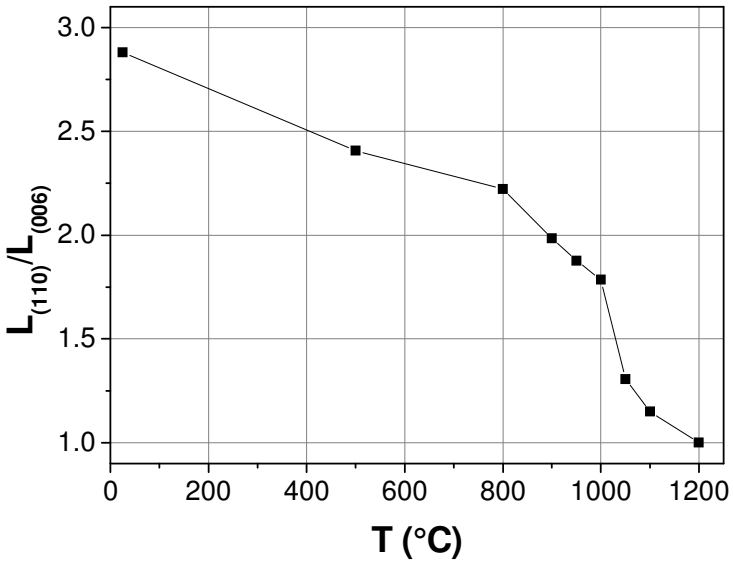

Figure S6. Variation of $L_{(110)}/L_{(006)}$ at different temperature of calcination for one hour.

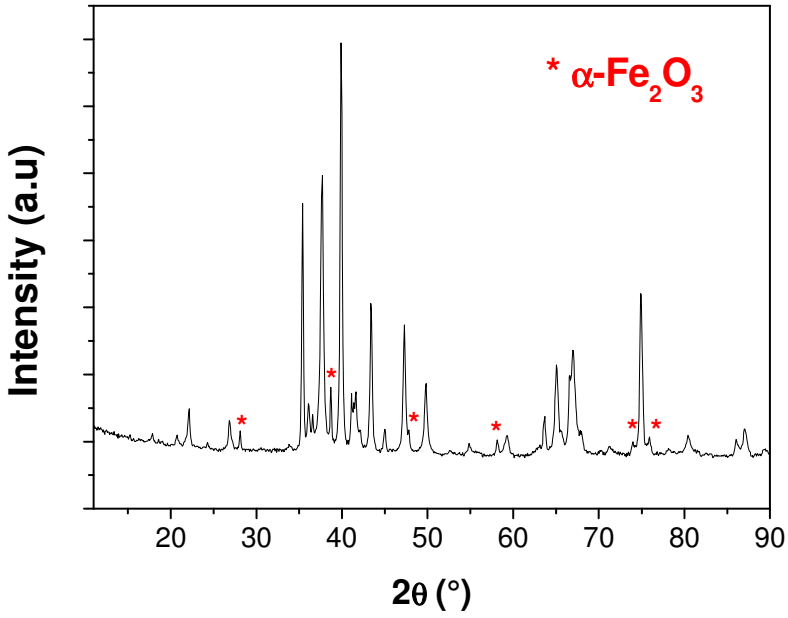

Figure S7. XRD pattern of a powder obtained by microwave heating for one hour at 200 °C a solution (pH = 10) of iron and strontium nitrates with a heating rate of 12 °C.min^{-1}.